J. COMBIN. MATH. COMBIN. COMPUT. 127a (2025) 8003--8025

Journal of Combinatorial Mathematics and Combinatorial Computing
www.combinatorialpress.com/jcmcc

Combinatorial Press

Deep Learning Based Peach Quality and Disease Detection Methods for Research in Intelligent Food Safety Detection

Yan Xiao[1,✉], Dongming Yao[2]

[1] *School of Engineering, Guangzhou College of Technology and Business, Guangzhou, Guangdong, 510850, China*
[2] *Guangdong Nonferrous Industrial Construction Quality Inspection Station Co., Ltd., Guangzhou, Guangdong, 510725, China*

ABSTRACT
With the rapid development of China's economic level and the significant improvement of people's living standard, the quality issue of peaches has become more and more strict. In this paper, based on deep learning algorithm, we propose the recognition method of peach fruit color, size and fruit shape features, combined with near-infrared spectroscopy detection technology, to quantify the peach fruit components and discriminate its maturity. Differential algorithm, standard normal transform, and multiple scattering correction are applied to pre-process peach fruit data. Based on M-YOLOv5s target detection framework, spectral analysis and image characterization techniques were used to jointly detect the degree of peach fruit disease. The distribution of peach fruit quality parameters was investigated, and the test results showed that 39.19% of the samples with measured values of fruit size were concentrated at 1.60-6.40 cm, and 61.79% of the samples with predicted values were concentrated at 2.50-7.50 cm, which was located at around the mean value of 4.763 cm.The classification accuracies of the information modeling set and validation set for the combination of the spectral analysis and image eigenvalue detection techniques were 91.439% and 88.487%, respectively, and the combined use of the two techniques had a high accuracy for the differentiation of diseased peach fruits. Based on the experimental results, the application of spectral detection technology in food freshness detection as well as pesticide residues and illegal additives is explored.

Keywords: Deep learning, Near-infrared spectral detection, Differential algorithm, M-YOLOv5s target detection, Diseased peach fruit

1. Introduction

Peach because of its fresh and delicious and rich in a variety of nutrients by many consumers, with the continuous improvement of living standards, consumers began to pay more and more attention to the peach quality, but the peach in the harvest, storage, transportation and other aspects of the operation

✉ Corresponding author.
E-mail address: xiaoyan9192@163.com (Y. Xiao).
Received 05 March 2024; Revised 20 April 2024; Accepted 05 December 2024; Published Online 15 April 2025.
DOI: 10.61091/jcmcc127a-440

will be improper or accidental damage, resulting in decay, in the production process susceptible to pests and diseases, thus affecting the quality of peach [1-4]. In order to solve this problem, it is necessary to test peaches, screen out damaged peaches, and improve the commodity quality of peaches [5].

In the detection of peach quality, if the use of manual judgment, it will be affected by the experience level of the inspector, which is subject to greater subjectivity, making the detection results uneven, and it is difficult to form a standardization [6-7]. Deep learning is popular in the field of target detection and identification due to its ability to extract global and local features of the target and its ability to extract features from a large amount of data, with obvious advantages in data processing. The properties of deep learning have received much attention in peach detection and pest recognition [8-11]. Deep learning is a type of representation learning is able to learn a higher level of abstract representation of the data and can automatically extract features from the data [12]. By pre-training the model, the features can be continuously adjusted and optimized, which can be used to process large amounts of data more quickly and easily, with better performance and higher accuracy [13-16]. Compared with detection techniques such as machine learning, deep learning shows more obvious advantages and provides technical support for realizing intelligent food safety detection [17-18].

Diseases produced during the growth process of peach will not only reduce the quality and yield of peach, but also affect people's dietary health, so timely and effective identification of peach diseases is the key to achieve disease control and then improve the quality of peach. Literature [19] designed a convolutional neural network (CNN) model capable of detecting peach product diseases and locating the diseased areas, which is beneficial in helping fruit farmers find treatments to protect peaches with a view to improving peach yields. Literature [20] used RGB images to assess multiple traits of peach fruits, including skin color, sugar content, and kernel splitting, and used a convolutional neural network (CNN) to classify and analyze these features, revealing that CNNs are able to efficiently diagnose a wide range of fruit traits and predict quantitative values from RGB images. Literature [21] reviewed peach quality nondestructive evaluation techniques such as machine vision technology and hyperspectral imaging, and evaluated the effectiveness of these techniques in assessing the internal quality, ripeness, and disease detection of peaches, describing the strengths and weaknesses of each technique for research in this field. Literature [22] proposed a peach disease detection method based on asymptotic nonlocal mean image algorithm and fusion of parallel convolutional neural network and limit learning machine with linear particle swarm optimization based on the problems of peach disease images and revealed the effectiveness of this method in peach disease detection. Literature [23] emphasized the importance of accurate identification of peach diseases and segmentation of diseased areas, and by applying deep network models (MaskR-CNN and MaskScoringR-CNN) to segmentation and identification of peach diseases, the model was able to obtain the name of the disease, its location, and segmentation, and achieve the output of detailed peach disease information.

Food safety detection is an important part of ensuring people's life and health, however, the traditional detection methods have relatively low iteration speed and cost-effectiveness, resulting in the emergence of food safety problems, which cannot meet the needs of modern industrial and commercial on the regulation, and AI, as a kind of cutting-edge technology, plays an important role in food safety detection. Literature [24] proposed a risk assessment method for dairy products based on ISM-AHP-RBF neural network and a loT-based method for milk production in dairy products, pointing out that ISM-AHP-RBF neural network can be rapidly iterated to a stable state and can accurately predict high-risk ingredients to ensure food safety. Literature [25] developed a novel multimodal optical sensing system aimed at intelligent food safety detection, which demonstrated the effectiveness of the system by identifying a variety of common foodborne bacteria that can be used in food safety inspections. Literature [26] examined the role of Al in strengthening food regulatory agencies, food safety and quality assurance systems, emphasizing that AI-driven automation and data analytics contribute to efficiency, accuracy, and real-time decision-making capabilities that improve food safety practices. Literature [27] points out that AI technologies in food safety are lagging behind in the area of commercial development due to the existence of barriers such as limited collaborative research and development efforts, and makes recommendations for the future such as improving data standardization and developing a collaborative ecosystem to enable the use of AI in food safety. Literature [28] proposed a unified Reinforcement Learning-Attention-Long and Short-Term Memory (RL-ALSTM) framework designed to address the challenge of food safety compliance prediction, which achieves highly accurate food safety prediction with excellent performance based on historical data and food-specific attributes.

In this paper, we identify the color of peach fruits by constructing an RGB color model and loading peach fruit images to map their information into HSV color space. The maximum transverse diameter of the peach is used as a basis for judging the size of the peach, and the roundness of the peach fruit is measured using the roundness method to measure the peach fruit shape. The near-infrared (NIR) spectroscopy technique was introduced, and the NIR spectroscopy data information was processed sequentially through the steps of abnormal sample rejection and reasonable division of sample set. The least squares regression algorithm was used to establish an internal quality prediction model for peach fruits, and the predicted values of the three quality indexes of peach fruits were obtained through the model to analyze the errors between the predicted values and the actual values. The spectra of three different maturity levels of peach fruits were averaged separately, and the corresponding spectra were plotted to discriminate the maturity level of peach fruits. Combining convolutional neural network and YOLO target detection algorithm, M-YOLOv5 target detection framework was constructed to recognize the degree of peach fruit disease.

2. Deep learning based peach fruit quality detection

2.1. Peach Fruit Color, Size and Fruit Shape Characteristics Extraction

2.1.1. Peach color identification. The HSV color space model and RGB color space model used for feature extraction of peach color. The peach image is first loaded and then mapped to the HSV color space, and the color type in the image is determined by performing statistics and operations on each channel component.

Figure 1 shows the RGB color model, which is a common color model based on the theory of three primary colors. It is widely used in real life, such as computers. Like the three primary colors, the RGB color model is made up of three colors: red, green and blue. According to the human vision characteristics, you can use R (red), G (green), B (blue) and other different ratios, thus R, G, B is what people call the three basic colors, white = 100% red + 100% green + 100% blue; purple = 100% red + 0% green + 100% blue. RGB color modes generally use three-dimensional axes to represent the values of individual channels.

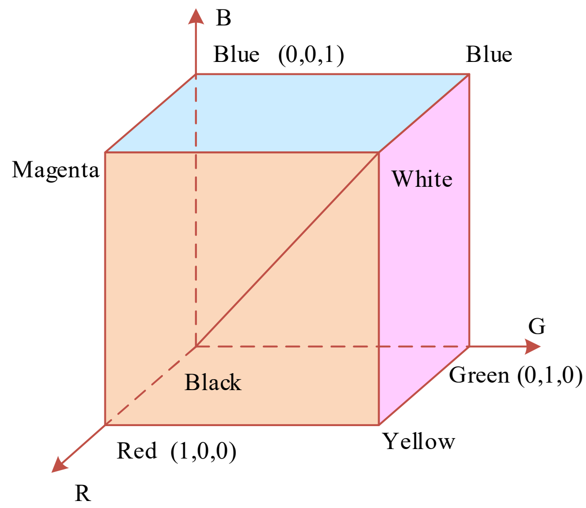

Fig. 1. RGB color model

The eight vertices of the square correspond to the eight base colors, i.e.: black (0, 0, 0) is the origin of the base colors, the three stereo intersection coordinates within the three coordinate system are red (1, 0, 0), blue (0, 1, 0), and green (0, 1, 0), and the rest of the three vertices are the coordinates of the three colors consisting of the three basic colors mixed together, red, blue, and green, composed of (1, 1, 1) colors.

Equal amounts of red, blue, and green mixed together to form (1, 0, 1) yellow, and equal amounts of green, blue, and green to form (1, 1, 1) colors, in which case the diagonal of the three basic colors of red, blue, and green indicates a change in the gray level of the image in the color space.

2.1.2. Peach size identification. The size of the peach has an important influence on the overall quality of the peach, and the size of the peach can be identified by extracting the amount of peach shape characteristics. The size of the horizontal diameter of the peach can best visualize the overall size of the peach. In the current market, the larger the peach, the higher the selling price, so this paper will eventually be the maximum diameter of the peach as a basis for judging the size of the peach.

In this paper, the methods of minimum outer circle and minimum outer rectangle are used to accurately measure the maximum cross diameter of peaches. These two methods are based on detecting the coordinates of the pixels at the outer edge of the peach, and selecting a few of them to form the smallest circle or the smallest rectangle that can accommodate the whole peach.

The background of the peach image acquired each time is a rectangular cardboard whose circumference is denoted by C. After a picture is taken with the camera, the total number of pixel points on the rectangle of the image is denoted by P. The corresponding coefficient K = C/P, which denotes the length of the true diameter corresponding to each pixel point of the captured image in mm, and the correlation coefficient K, which was obtained by using several image trials and multiple calculations, is approximately 0.00224.

2.1.3. Peach fruit shape identification. The roundness was measured by the roundness method and the validity of the method was verified experimentally. The circularity value metric is expressed as equation (1):

$$metric = \frac{r_s^2}{r_l^2} = \frac{S/\pi}{L^2/\left(4\pi^2\right)} = \frac{4\pi S}{L^2} \tag{1}$$

where S denotes the region of roundness, r_s denotes the radius of the circle obtained accordingly,

L denotes the circumference of the circle, and r_L denotes the diameter of the circle obtained accordingly. The results showed that the shape of the fruit tended to be rounded as the roundness of the fruit increased, and its calculation of the number of roundness tended to be 1. Therefore, the roundness of the peach was classified according to its roundness size.

Using the improved analysis method of roundness value, on the basis of the original roundness variance, the roundness value of peach multi-image was obtained by experimental method, and its mean and variance were calculated, and the larger roundness variance was obtained. The results show that the larger the mean and the smaller the variance of this roundness value, the larger its roundness is and the better its roundness is. The specific implementation process of this method is as follows: by processing the binary image, the pixel perimeter and pixel area of the binary image are obtained, so that the roundness of the image can be calculated, and then the mean and the variation of the roundness are obtained, the mean value of the roundness is compared with the roundness of the fruit type, and the variance is compared with the determined critical value, and the fruit type grading of the crisp peaches is obtained. In this paper, the roundness value analyzer is linked to the variance method, because it is used to measure the volatility of a set of data, when a peach has a better roundness and is closer, the greater the value of roundness on all surfaces of the crisp peach, the closer to 1, the more the variation tends to be 0. The result of calculating with the algorithm is that the greater the mean value of roundness, the smaller the variance, the greater the roundness, the higher the grading level of the fruit.

2.2. Peach maturity discrimination model by NIR spectroscopy

2.2.1. Near-infrared spectroscopic detection techniques. The process of near-infrared spectroscopy analysis consists of two major steps: one is to establish a calibration model based on the measured data and spectral data of the calibration set samples and to test and optimize the model, and the other is to use the established analytical model, based on the near-infrared spectra of the unknown samples, to quantitatively predict the content of the relevant components in the unknown samples, or qualitatively discriminate the category of the unknown samples [29]. The specific analysis process is shown in Figure 2.

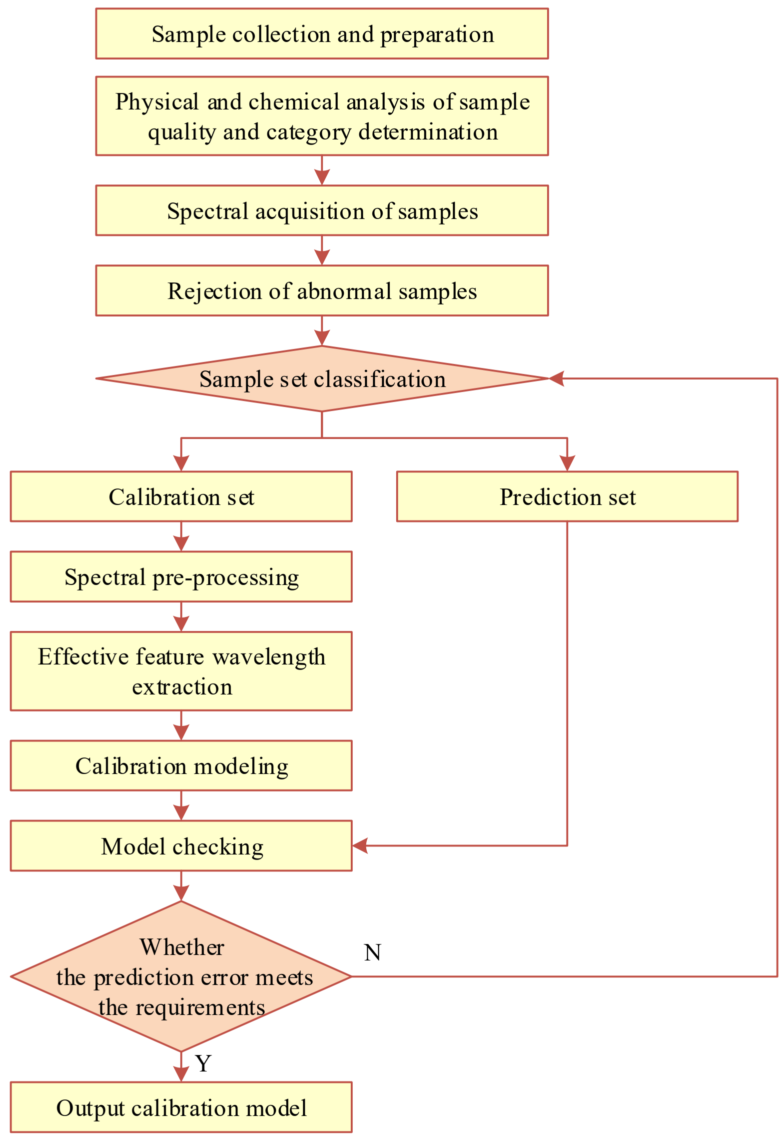

Fig. 2. General process of NIR analysis

2.2.2. Evaluation criteria for NIR spectral analysis models. The correlation coefficient R indicates the proportion of the regression sum of squares to the total sum of squares, and the closer it is to 1 the closer the predicted concentration value is to the true value:

$$R = \sqrt{\left(1 - \frac{\sum_{i=1}^{n}\left(Y_i - \overline{Y_i}\right)^2}{\sum_{i=1}^{m}\left(Y_i - Y_m\right)^2}\right)} \times 100\% \tag{2}$$

where n is the number of samples, Y_i is the true value of the i rd sample, Y_m is the average of the true values of the samples, and $\overline{Y_i}$ is the predicted value of the i th sample.

Root Mean Square Error of Correction (RMSEC) and Root Mean Square Error of Prediction (RMSEP) The smaller the values of RMSEC and RMSEP of the analytical model the better the predictive performance of the model:

$$RMSEC = \sqrt{\frac{1}{n_c}\sum_{i=1}^{n_n}\left(\hat{y}_i - y_i\right)^2} \tag{3}$$

$$RMSEP = \sqrt{\frac{1}{n_p}\sum_{i=1}^{n_i}\left(\hat{y}_i - y_i\right)^2} \tag{4}$$

where: n_c is the number of samples in the calibration set, n_p is the number of samples in the prediction set, $\hat{y}_i$ is the predicted value of the i th sample, and y_i is the measured value of the i th sample.

2.2.3. NIR spectral data processing methods:

1) Abnormal sample rejection. The so-called anomalous samples (also known as odd samples) refer to the samples with large errors in the measured concentration or spectral data. Among them, the error of measured concentration is mostly caused by improper selection of measurement method or human subjective factors; the error of spectral data is mainly due to the stability of the spectrometer itself, inappropriate sample pre-treatment methods, and the influence of environmental factors.

2) Reasonable division of sample set:

(1) Concentration gradient method. Concentration gradient method is one of the most commonly used conventional sample set division method, first of all, by the samples in accordance with the proposed determination of the concentration of components from high to low (or vice versa) for the arrangement, and then a certain proportion of samples from the order of the composition of the calibration set and prediction set. Although this method is simple, intuitive and easy to realize, it fails to take into account the influence of the sample spectral data on the sample, which often makes the correction set of samples less representative.

(2) Kennard-Stone method. Kennard-Stone method by the spectral difference (the farthest distance from the European style) of the sample selected into the correction set, while the rest of the more similar samples are put into the prediction set, to effectively ensure that the representative samples into the correction set, and thus maximize the distribution of samples in the correction set is uniform and consistent. This method is a machine identification method, which does not take into account the fact that some spectral differences are not entirely caused by differences in the composition or properties of the measured samples, the computational volume is large, and there is a possibility that anomalous samples are also selected into the correction set.

(3) X-Y Symbiotic Distance Algorithm. The SPXY method is a new sample set division method developed based on the Kennard-Stone method, which simultaneously takes into account the Euclidean distance between the absorbance value and the concentration of each sample, so that the selected samples in the calibration set are targeted at a particular composition, which can fully ensure that the information of the samples in the calibration set adequately covers the samples in the prediction set, and make the sample set selected for division The calibration set is more representative of the predicted samples.

2.2.4. Pre-processing methods for NIR spectra:

1) Derivative (differential) algorithm. The first-order and second-order derivatives of the spectrum are commonly used in near-infrared spectral analysis of the baseline correction and spectral resolution preprocessing methods, which can effectively eliminate the interference of the baseline and

other backgrounds, distinguish overlapping peaks, and improve the resolution and sensitivity. There are two general methods for spectral derivation: direct difference method and Savitzky-Golay method. The direct difference method is suitable for high-resolution, dense wavelength distribution of the spectrum, while the Savitzky-Golay method for sparse wavelength sampling points of the spectrum has better results.

2) Standard Normal Transform Algorithm. The standard normal transform (SNV) is mainly used to eliminate the effects of solid particle size, surface scattering, and light-range changes on the near-infrared diffuse reflectance spectra, etc. The SNV algorithm achieves the processing requirements by transforming the spectra of each sample in accordance with Eq. (5):

$$X_{i,SNV} = \frac{X_{i,k} - X_i}{\sqrt{\frac{\sum_{k=1}^{m}\left(X_{i,k} - X_i\right)^2}{(m-1)}}} \tag{5}$$

where X_i is the average of the spectra of the i nd sample, $k = 1, 2, \ldots m$, m are the number of wavelength points: $i = 1, 2, \ldots n$, n are the number of samples in the correction set.

3) Multiple scattering correction algorithm. The purpose of multiple scattering correction (MSC) is basically the same as that of SNV, which is to eliminate the scattering effects of uneven particle distribution and particle size [30].

2.2.5. Effective Eigenwave Number Optimization. PLS algorithms can be divided into: ordinary interval-biased least squares, joint interval-biased least squares, backward interval-biased least squares and moving window least squares according to the principle of implementation of specific methods [31]. The ordinary interval partial least squares algorithm first divides the spectral interval of the whole band into several interval intervals of equal width, and then participates in the PLS modeling with the spectrum of each interval interval, and then establishes the root mean square error (RMSECV) by comparing the interaction of each interval interval to establish the model, and selects the optimal interval interval according to the RMSECV value, while several other methods are based on the ordinary interval partial least squares method and are improved to a certain extent.

The UVE algorithm is a more intuitive and practical method of selecting eigenwave numbers based on PLS regression coefficients b that integrates noise and concentration information. The basic principle is that in the PLS model, the spectral matrix X and the concentration matrix Y have the following relationship:

$$Y = X\mathrm{e} + \mathrm{b} \tag{6}$$

where b is the coefficient vector and e is the error vector.The UVE method, on the other hand, builds a PLS cross-validation model by adding a certain number of random variables to the spectral matrix, and then analyzes the stability of the quotient of the mean and the standard deviation of the coefficient vector b, t, viz:

$$t_i = \frac{mean\left(b_i\right)}{S\left(b_i\right)} \tag{7}$$

2.2.6. Corrective modeling. The PLSR method, based on PCR, decomposes both the spectral matrix X and the concentration matrix Y, and strengthens the correlation between them during the decomposition, thus ensuring that the best calibration model is obtained. The model realization process is mainly as follows:

Firstly, the spectral matrix X and concentration matrix Y are decomposed at the same time, and the model is:

$$X = TP + E \tag{8}$$

$$Y = UQ + F \tag{9}$$

where T and U are the score matrices for matrices X and Y, respectively, P and Q are the loading matrices for matrices X and Y, respectively, and E and F are the residuals matrices for the PLSR fits for matrices X and Y, respectively.

In the second step, linear regression analyses for T and U were performed:

$$U = TB \tag{10}$$

$$B = \left(T^{\mathrm{T}}T\right)^{-1} T^{\mathrm{T}}Y \tag{11}$$

In the third step, the score T_{Unknown} of the spectral matrix X_{Unknown} of the unknown sample is firstly derived from P, and then the concentration prediction is obtained from the following equation:

$$Y_{\mathrm{Unknown}} = T_{\mathrm{Unknown}} BQ \tag{12}$$

2.3. Peach quality test results

2.3.1. Removal of outlier samples. In the determination of chemical index values due to human operation, temperature, humidity and spectral acquisition may produce some abnormal data, these abnormal samples will affect the establishment of the model, and thus need to remove these samples, in this paper, using the t-test criterion, the abnormal samples one by one to remove, and using SPSS 18.0 to further validate the abnormal value of its, respectively, the fruit size, SSC and fruit shape indicators 360 The outliers of 360 spectral predictions of fruit size, SSC and fruit shape were removed, and the sample capacity, number of outliers and number are shown in Table 1.

SSC measured values ranged from 10.615% to 16.425% (Mean = 12.736, SD = 1.036), and predicted values ranged from 11.268% to 16.185% (Mean = 13.468, SD = 0.965). The measured mean and standard deviation of fruit size were 6.016 and 2.755, respectively, and the predicted mean was 4.763 with a standard deviation of 2.036. The measured values of fruit shape were in the range of 4.865 to 5.725, and the predicted values were in the range of 4.826 to 5.436. For the coefficients of variation, the coefficients of variation for the measured and predicted values of SSC were 7.93 and 6.78%, respectively, and for the predicted values of fruit shape, the coefficients of variation were 3.0 and 3.0%, respectively. For the coefficient of variation, the coefficients of variation of the measured and predicted values of SSC were 7.93% and 6.78%, respectively; the coefficients of variation of the measured and predicted values of fruit shape were 3.42% and 2.36%, respectively, which were less than 10%, and were weak. The coefficients of variation of measured and predicted fruit size were 45.75% and 43.69% respectively, which were greater than 30%, significantly higher than the SSC and fruit shape, which were strong variations. From the preliminary observation of the above results, it was found that the distribution of measured and predicted quality parameters was similar.

Table 1. Statistics of different quality indices

Parameters	Soluble solid content SSC/%		Fruit size(cm)		Fruit shape	
	Measured	Forecast	Measured	Forecast	Measured	Forecast
Sample capacity (exception) N	348	348	358	358	354	354
Number of abnormal values (numbered N)	5(20, 25, 70, 75, 85)		6(215, 233, 278, 115, 293, 302, 316)		10(18, 156, 175, 177, 192, 248, 275, 283, 293, 302)	
Min	10.615	11.268	1.466	0.096	4.865	4.826

Max	16.425	16.185	12.234	10.958	5.725	5.436
Mean	**12.736**	**13.468**	**6.016**	**4.763**	**5.236**	**5.125**
SD	1.036	0.965	2.755	2.036	0.185	0.126
R	5.869	5.035	10.765	10.865	0.936	0.612
CV	7.93%	6.78%	45.75%	43.69%	3.42%	2.36%

2.3.2. Internal quality prediction modeling. Non-destructive techniques take the lead in rapid detection of different sample qualities, ease of installation and continuous determination compared to traditional destructive methods. NIR spectroscopy is currently the most commonly used spectral analysis technique due to its non-destructive, rapid, efficient and environmentally friendly characteristics, objective measurements and high accuracy, and is particularly suitable for fruits and vegetables in the NIR range of 700 to 2 500 nm. In this study, fruit quality of "Shenzhou Peach" at harvest time was examined using SACMI nondestructive equipment (wavelength range of 600-1000 nm).

The least squares regression algorithm was used to establish correction models for SSC, fruit size, and fruit shape and to obtain the predicted values of the three quality indexes through the models. Figure 3 shows the correlation between the measured and predicted values of internal quality of fruit, with SSC in Figure (a), fruit size in Figure (b) and fruit shape in Figure (c). The correlation coefficients between measured and predicted values of internal quality were calculated, and the measured and predicted values of peach fruit SSC showed a highly linear positive correlation ($R^2 = 0.81471$, $p < 0.01$), SEP = 0.4633. Peach fruit size measured and predicted values were also significantly and linearly positively correlated, with an R^2 of 0.38259, P less than 0.01, and a SEP value of 2.0248. Peach fruit shape measured values were also significantly and linearly positively correlated with predicted values, with an R^2 of 0.41366, P less than 0.01.

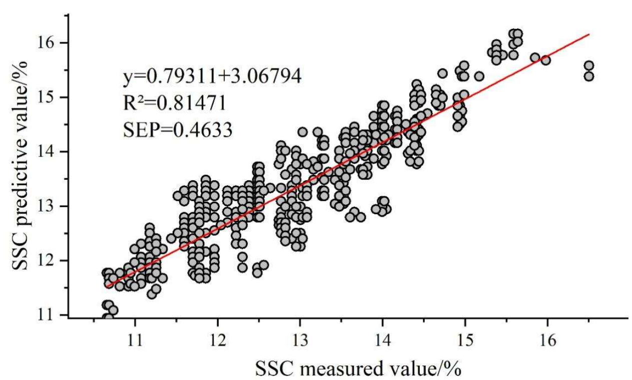

(a)SSC

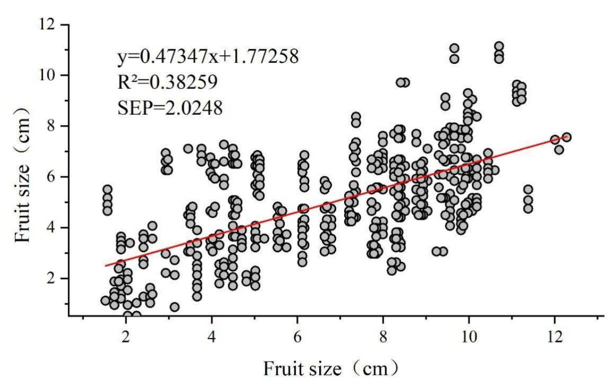

(b)Fruit size

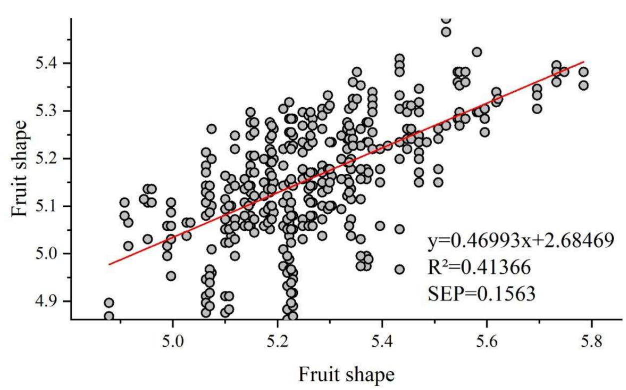

(c)Fruit shape

Fig. 3. The correlation between the measured value of the fruit and the predicted value

2.3.3. Distribution of quality parameters. Figure 4 shows the distribution of measured and predicted values of SSC, fruit size and fruit shape, with SSC in Figure (a), fruit size in Figure (b) and fruit shape in Figure (c). Among them, 47.6% of the samples with measured SSC values were concentrated in the range of 11.6% to 13.4%, which was located around the mean value of 12.736%, and 58.08% of the samples with predicted SSC values were concentrated in the range of [12.4%, 14.4%], which was located in the range of the mean value of 13.468%. Fruit size measured values of 39.19% of the samples ranged from 1.60 to 6.40 cm, and fruit size predicted values of more than 60% of the samples were concentrated in the range of 2.50 to 7.50 cm.

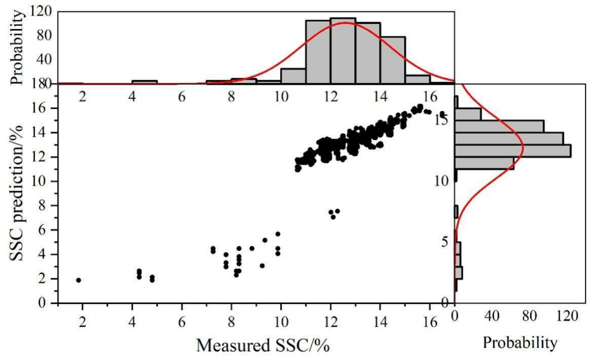

(a)SSC

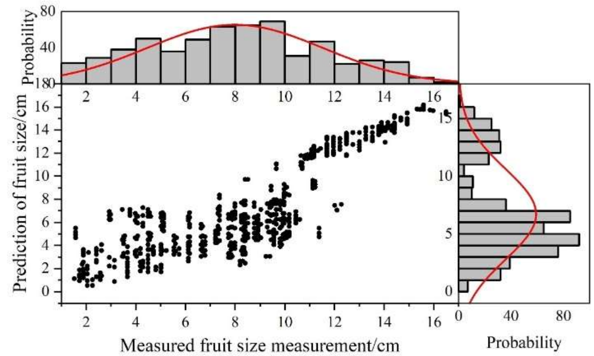

(b)Fruit size

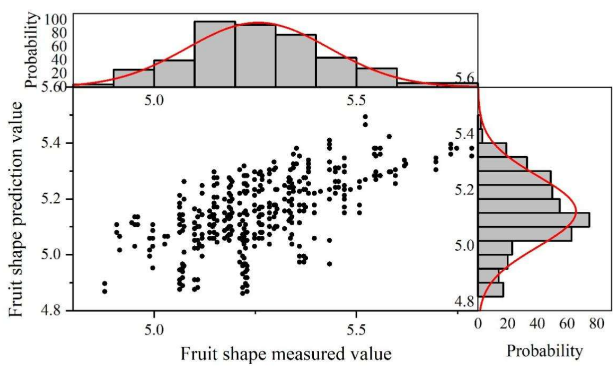

(c)Fruit shape

Fig. 4. SSC, fruit size and fruit shape and predictive value distribution

2.3.4. Peach fruit maturity analysis:

1) Average spectra of maturity. The spectra of three different maturity levels of peach fruits were averaged separately and the corresponding spectra were plotted. As shown in Fig. 5, the peaks and valleys in the 4500-8500 cm^{-1} wave number show obvious differences, and the absorbance has a great difference, in the 5000 cm^{-1} wave number, the absorbance is around 0.9-0.9935, while in the 6750 cm^{-1} wave number, the absorbance is in the 0.745-0.806 range. This is mainly due to the existence of a certain degree of chlorophyll ring-breaking in the epidermis of peach at different picking periods, and the different degree of changes in the internal quality of peach.

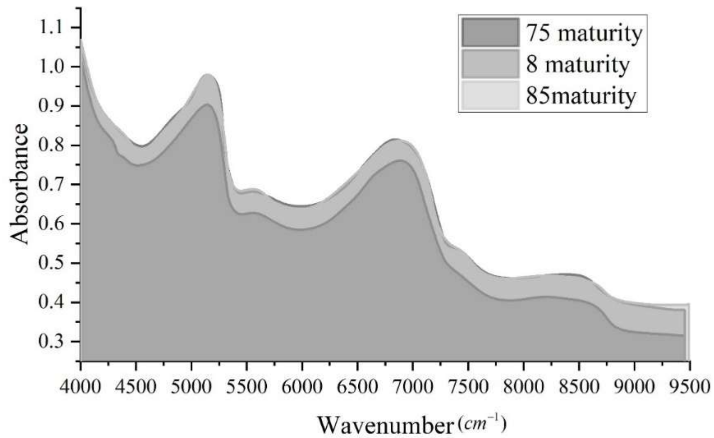

Fig. 5. Average spectra of samples of different maturity

2) Spectral principal component analysis. Figure 6 shows the scores of the first three principal components, there is a clear distinction between different ripeness levels of peach, but there is also a small part of the overlap, 75 ripeness of the principal components of the main concentration range between (-5, -2), (-0.2, 0.4), (-3, 1) The cumulative contribution of the first three principal components PC1 + PC2 + PC3 was 67.953%.

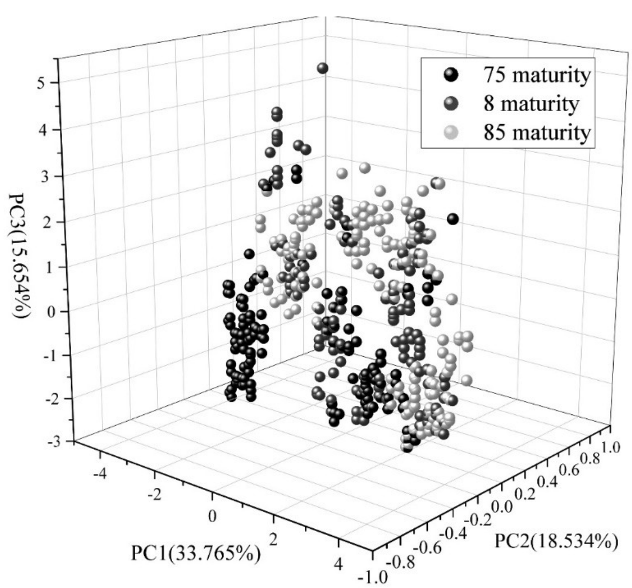

Fig. 6. The top 3 main components score

3. Deep learning based disease detection method for peach trees

3.1. Convolutional Neural Networks

3.1.1. Network structure:

1) Convolutional Layer. The role of the convolutional layer is to learn and extract features from the input image. The core of **the** operation of this layer lies in the convolution kernel, which can perform convolution operations on different feature maps, and a new feature map is obtained by the convolution kernel of the layer after convolving the input of the upper layer. In the feature extraction process, low-level features such as lines and edges in the image are extracted by the shallow

convolutional layer, and as the convolutional kernels are stacked, the abstract information of the image is extracted by the deeper convolutional layer.

2) Pooling layer. Pooling layer is also called downsampling layer, which is needed to perform feature dimensionality reduction through pooling layer after feature extraction. The pooling operation not only reduces the number of parameters in the training process, but also prevents the generation of overfitting. The common pooling operations are maximum pooling and average pooling. Maximum pooling is to select the maximum value of a region on the feature map to represent the region, mainly extracting the texture information in the feature map. Average pooling is to take the average value of a region on the feature map, mainly extracting the background information in the feature map.

3) Fully Connected Layer. After a number of convolution and pooling operations to reach the fully connected layer, all neurons in the fully connected layer are connected to all neurons in the previous layer, the purpose is to synthesize all the features learned earlier and transform the 2D feature map into a 1D vector to achieve classification.

3.1.2. Regression-based target detection. Regression-based target detection algorithms do not generate candidate regions and can predict the bounding box location and the class of the target directly in the input image, with a simpler network structure and faster detection speed. Regression-based target detection algorithms mainly include YOLO, SSD and RFBNet.

YOLO first adjusts the image size to 418×418 uniformly in the detection process and divides the image into 7×7 grids, extracts the features of the input image by convolutional neural network, and predicts the bounding box of the target and the category confidence in each grid. Finally, the prediction box is filtered by non-maximal suppression method.YOLO uses end-to-end training and treats the detection problem as a regression problem, which improves the detection speed.

The regression-based target detection contains only one detection process, the model structure is simple and small, the computational efficiency is higher, with the continuous improvement of the model, it can improve the detection speed and also ensure that the detection accuracy remains unchanged, which provides the conditions for the model to be transplanted to mobile devices.

3.2. Peach fruit disease recognition method based on M-YOLOv5

3.2.1. Peach fruit dataset. In this chapter, peach fruits were used as the research object, and the image collection was completed in a peach orchard in Shandong Province, with a total of 4027 test data collected. The test data were categorized into four groups according to their disease types: healthy peaches, anthracnose peaches, brown rot peaches, and scab peaches. Among them, there were 1565 healthy peaches, 879 anthracnose peaches, 801 brown rot peaches, and 782 scab peaches, and some images of this dataset were captured by Xiaomi 9 cell phone on peach trees. At the same time, in order to enhance the robustness and generalization of the data, this paper adds peach disease images taken in other backgrounds, and the pixels of the collected images are uniformly 4000×3000, and the collected experimental data are divided into the training set and the test set according to the ratio of 7:3 and saved as a TXT file with the location and category information after being annotated one by one using an image annotation tool, as the peach fruit disease dataset. In order to enhance the generalization ability of the model, this section continues to expand the dataset using offline data enhancement methods such as rotational changes, color dithering, etc., and the expanded dataset is expanded from 4,027 to 12,081 images.

3.2.2. M-YOLOv5s Target Detection Framework. Aiming at the problems of deep learning model occupying large memory demand, high detection latency and unable to adapt to the demand of accurate identification of small target disease areas of peach fruits, this section selects the regression-based single-stage target detection algorithm YOLOv5s to identify and detect the existence of diseases in peach fruits.There are abundant redundant features in YOLOv5s to ensure the model's generalization ability, which is characterized by low complexity of network and high real-time characteristics of Mobileone network introduced into the Backbone part to achieve feature extraction for peach fruit diseases, In this regard, Mobileone network with low network complexity and high real-time performance is introduced into the Backbone part of YOLOv5s to realize the feature extraction of peach fruit diseases. With the deepening of the network, the small-scale disease features of peach fruits are no longer prominent, in order to enhance the learning ability of the network on the channel, the channel attention (SE) is added to the Mobileone module to improve the effective extraction of small target disease features. For the case of multi-scale disease in peach fruits, the feature pyramid network and path aggregation network are fully utilized to fuse the feature information of different scales, so that the model can achieve better prediction effect. Through the above improvements, the M-YOLOv5s network model was finally constructed, and the structure of M-YOLOv5s is shown in Figure 7.

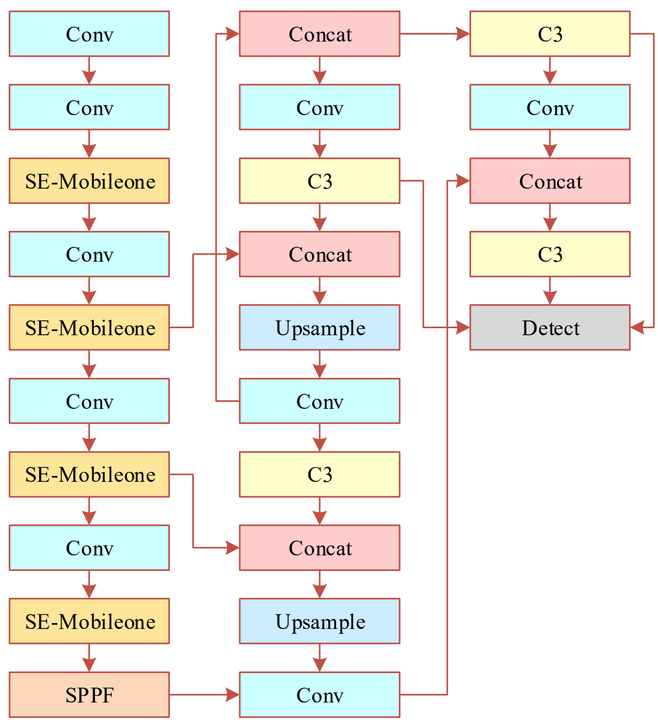

Fig. 7. Improved M-YOLOv5s structure diagram

3.2.3. Mobileone module. Mobileone network is characterized by high real-time and low complexity, which is very suitable for the application of edge devices in agriculture, so this chapter uses Mobileone structure to replace the backbone network part of YOLOv5s in order to extract the features. As a low-latency lightweight network model, Mobileone network, in order to save the cost of data movement to avoid the memory bottleneck problem, absorbed the idea of heavy parameterization in the inference process, and changed the multiple branching to use the single branching architecture, to reduce the latency cost brought by the efficient architecture. In terms of controlling model parameters, Mobileone follows Mobilenet in using depth separable convolution, i.e., replacing ordinary convolution in deep convolutional neural networks with deep convolution and point-by-point convolution to promote information fusion between different channels.

3.2.4. Channel Attention Module. The core idea of SE-Net is to utilize a fully connected network to learn feature weights based on loss function values. As the main structure of SE-Net, the channel attention module enables the convolutional neural network to have better expressiveness by continuously training the network model in order to learn the important regions, so as to quickly extract the important features of the image and their dependencies. In the detection task of peach fruit diseases, there are some disease targets with small regions and insignificant features, which can easily cause problems such as wrong detection and missed detection. In order to improve the detection accuracy of the model the SE attention module is added to the Mobileone module to form the SE-Mobileone module, which enhances the learning ability of the important channels to realize the effective extraction of the features of interest of peach fruits.

3.2.5. Threshold gradient descent method. Although the performance of the improved YOLOv5s model has been greatly improved, it still suffers from the problems of model instability and slow convergence. To solve the above problems, this paper proposes the threshold gradient descent method. That is, if the gradient update value is small in the current iteration, the secondary gradient descent (SeGD) method is used, so as to increase the gradient update value of the current iteration. If the gradient value is large in the current iteration then Compensated Gradient Descent (CGD) algorithm is used, which decreases the gradient update value of the current iteration. And when the gradient update value is normal in the current iteration then stochastic gradient descent is used and the computer performs the normal iteration steps. In the secondary gradient descent method the first gradient descent uses Adam optimizer with the following formula:

$$m_t = \beta_1 m_{t-1} + \left(1-\beta_1\right) g_t \tag{13}$$

$$V_t = \beta_2 V_{t-1} + \left(1-\beta_2\right) g_t^2 \tag{14}$$

$$g_t = \nabla f\left(w_t\right) \tag{15}$$

where t is the current training round, β_1 and β_2 are the two hyperparameters in the Adam optimizer, g, is the gradient at round t. m_t, is the momentum at round t, and V_t is the second-order momentum at round t. Although the Adam optimizer has great progress compared with other optimizers such as SGD, in some cases where the image color is more complex, the single gradient descent optimization is difficult to find the optimal loss function and there may be problems such as slow operation of the program and long convergence time. On this basis, this paper introduces the secondary gradient descent algorithm, that is, the SGD optimizer is introduced after the Adam optimizer, at this time the update gradient is:

$$g_t = \nabla\left(\nabla f\left(w_t\right)\right) \tag{16}$$

In the improved formula is as follows:

$$m_{t+1} = \beta_1 m_t + \left(1-\beta_1\right)\left(\nabla\left(\nabla f\left(w_t\right)\right)\right) \tag{17}$$

$$V_{t+1} = \beta_2 V_t + \left(1-\beta_2\right)\left(\nabla\left(\nabla f\left(w_t\right)\right)\right)^2 \tag{18}$$

The gradient descent formulas before improvement are shown in (13), (14) above and after improvement the gradient descent formulas are shown in (17), (18) above. The improved algorithm increases the time complexity to a certain extent, but the faster finding of the optimal solution reduces the overall running time of the algorithm, the following is the pseudo-code for the quadratic gradient descent.

When the gradient update value is small, this paper uses the compensated gradient algorithm for gradient update, where:

$$g_t = \nabla f\left(w_t\right) + lr * \left(\nabla f\left(w_t\right) - \nabla f\left(w_{t-1}\right)\right) \tag{19}$$

The gradient update value of the model is increased by adding the gradient difference between the current iteration and the previous iteration in the current iteration. The following algorithm (20) shows the pseudo-code of the compensated gradient algorithm. The gradient descent method used in this paper is determined in terms of the inter-gradient value, defining the update value Th as:

$$Th = \frac{Loss(t)}{4\|g_1\|} \tag{20}$$

where $Loss(t)$ is the loss function for backpropagation in this iteration, $\|g_t\|$ is the number of paradigms for gradient updating in this iteration, when Th is less than the dynamic threshold then SeGD is used to increase the update value of gradient in the current iteration, when Th is greater than the dynamic threshold then CGD is used to decrease the update value of gradient in the current iteration, and when the update value is normal then normal batch updating is used with SGD:

$$\begin{cases} SeGD, if\ Th \le Loss(t-1) - Loss(t) / \|g_1 - g_{t-1}\| \\ CGD, if\ Th \ge Loss(t-1) - Loss(t) / \|g_t - g_{t-1}\| \\ SGD, other \end{cases} \tag{21}$$

3.3. *Peach fruit disease detection results*

In order to detect peach fruits at different disease stages, two thirds of the data were used for modeling and the other one third of the data were used for validation, in this chapter, the Partial Least Squares Discriminant Approach (PLS-DA) was utilized to build a differentiation model, in addition to the identification of different kinds of fungal diseases, which was also done with the PLS-DA model. Ultimately, the effects of spectral and image information on disease recognition and differentiation, as well as the recognition of different stages of disease, are compared. The experiment was divided into three experimental groups of 270 decay samples and 30 control samples of healthy peach fruits, namely, Aspergillus gray staphylococcus (*B.cinerea* abbreviated as B. c), Rhizopus stolonifera (*R.stolonifer* abbreviated as R. s), and Anthracnose (C. a abbreviated as C. a).

3.3.1. Spectral analysis. Figure 8 shows typical reflectance spectra of peach fruit under different decay conditions. Figure 8(a) shows the average spectra for different stages of decay and for the control group, and Figure (b) shows the average spectra for each treatment group and for the control group. "all" represents the average spectra of a total of 270 decay samples in the three experimental groups, and "CK" refers to the average spectral value of 30 healthy peach fruits, which are calculated from 90 samples (30 per fungal disease group) for the three different decay stages, without considering different fungal diseases. In figure (a), there is an absorption peak at 665nm of the spectrum where there is a significant difference between diseased and healthy peach fruits. 665nm is reported to be the absorption peak of chlorophyll, which has been reported in fruits such as peach fruits. At the absorption peak of chlorophyll, the spectral reflectance values of peach fruits in the treatment group were significantly lower than those of healthy peach fruits in the control group, and the relative reflectance values of healthy peach fruits ranged from 0.7 to 0.97 after the wavelength of 700. The possible explanation is that when the fungus grows and multiplies within the peach fruits, the cellular structure is ruptured, allowing chlorophyllase to appear simultaneously with chlorophyll, resulting in an accelerated decomposition of ensiled chlorophyll. The spectral difference between decayed and healthy samples increased as the level of decay increased, making it easy to distinguish decayed samples based on spectral differences during periods of severe decay. According to Fig. (a) it can be found that there is a significant difference in the spectra between the treatment group samples and the healthy samples, and it can be considered to use the spectra to categorize the decayed peach fruits and the healthy peach fruits. After comparing the spectra of peach fruits in the treated and healthy groups, the next step will be to investigate the differences between the different treatment groups. Figure (b) shows the average spectral plots for each treatment group and the control group, and the average spectra were calculated from the ROIs of 90 samples for each of the three treatment groups. The spectral reflectance of the three treatment groups was lower than that of the control group at 560-660 nm and 700-800 nm wavelengths, and the spectral reflectance of the control group was lowest at the chlorophyll absorption peak around 665 nm.

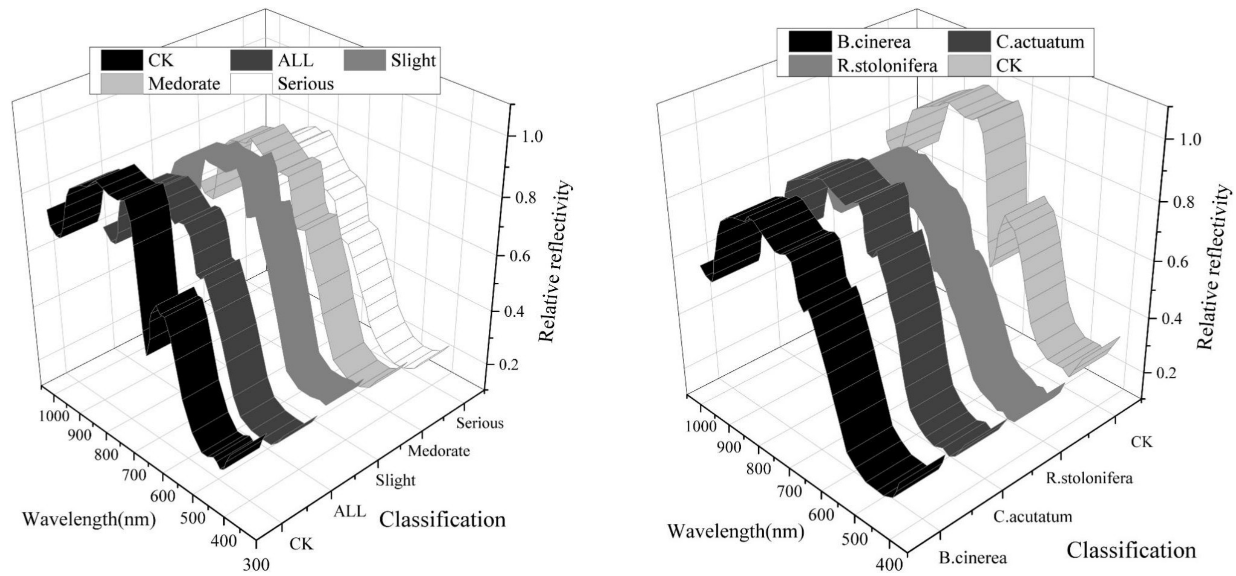

(a)The average spectrum of different decay stages and the control group

(b)The average spectrum of the control group and the control group

Fig. 8. The typical anti-ejaculation spectrum of peach fruit in different decay

3.3.2. Image eigenvalue analysis. In order to obtain more image features, image gray scale features are extracted as shown in Fig. 9.PCA provides an effective method to reduce the hyperspectral dimensions, enhance the information of interest and eliminate the noise. In the study of this chapter, the images of full band (400-1000 nm) were analyzed by PCA, and the first principal component map can better show the information of lesions, meanwhile, it can eliminate the effect of other colors of epidermis. Then the grayscale histogram and GLCM texture features are extracted from the image of the first principal component, and the grayscale histogram shows that the grayscale values are mainly concentrated between 0 and 0.1, and a little after 150 the grayscale values are around 0.2 to 0.87.

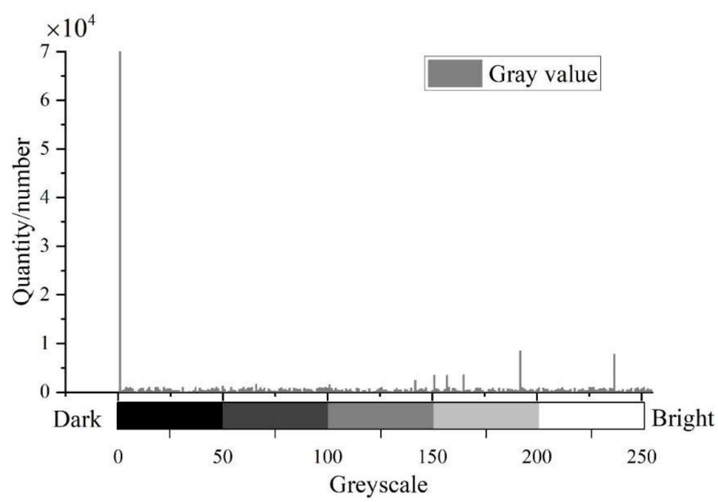

Fig. 9. Gray histogram

3.3.3. Diseased peach fruit differentiation. In order to fulfill the most basic requirements, infected peach fruits had to be identified and selected. Firstly, all samples were divided into two categories - diseased peach fruits and healthy peach fruits, diseased peach fruits included all three diseases under mild, fair and severe diseases.

The classification PLS-DA models of diseased and healthy peach fruits were built using full band information (420 bands), image information (38 features) and combined information 458 features respectively, and the classification results are shown in Table 2, MS is the modeling set and VS is the validation set. Table 2(a) shows the classification results of differentiating only the experimental group (diseased peach fruits) and the control group (healthy peach fruits) without considering the decay stage, and the PLS-DA model has high classification accuracy for both spectral and image features, especially the spectral information model. The classification model for the mildly diseased group (Table (b)) showed relatively poor results compared to the other decay stages, with classification accuracies of 91.439% and 88.487% for the modeling and validation sets of the combined information, respectively. As can be seen from Tables (a)-(d), the model based on combined features can slightly improve the classification accuracy.The results of the PLS-DA model show that diseased peach fruits can be easily distinguished from healthy peach fruits, whether based on spectral information or image features.

Table 2. The classification results of the PLS-DA model

Disease level	Rank	Spectral feature		Image feature		Spectral image	
		MS	VS	MS	VS	MS	VS
(a)All	Disease	98.841	97.785	94.552	94.425	99.436	98.826
	Health	100	100	100	100	100	100
	Subtotal	99.421	98.893	97.276	97.213	99.718	99.413
(b)Slight	Disease	86.636	83.315	83.315	81.245	88.315	86.625
	Health	95.515	91.136	90.326	90.035	94.563	90.348
	Subtotal	91.076	87.226	86.821	85.64	91.439	88.487
(c)Normal	Disease	100	100	100	90.245	100	100
	Health	100	100	100	100	100	100
	Subtotal	100	100	100	95.123	100	100
(d)Serious	Disease	100	100	100	100	100	100
	Health	100	100	100	100	100	100
	Subtotal	100	100	100	100	100	100

3.3.4. Distinguishing between different fungal diseases. In order to achieve higher classification requirements, this subsection will classify different fungal diseases.The PLS-DA algorithm establishes classification models based on spectral information, image information and combined information, respectively.Table 3 shows the classification results of the PLS-DA model for peach fruits with different disease levels based on spectral and image information.The classification results of different disease levels of peach fruits were summarized as follows: B. gray staphylococcus (*B.cinerea* abbreviated as B. as B. c), Root Mold of Creeping Sap (*R.stolonifer* abbreviated as R. s), and Anthracnose (C. a abbreviated as C. a). Similar to Table 2, all samples were first differentiated, followed by a separate discussion of the classification effects of different decay stages. As far as the modeling results of spectral information are concerned, (I) the classification accuracies of the prediction sets for each dataset are higher than 90% without considering the decay stages. Among them, the classification accuracies of diseases caused by *B.cinerea* and *C.acutatum* were much lower than those of healthy samples. The classification accuracy of healthy peach fruits was almost 100% (except for the spectral feature validation set which was 90.455%), which implies a strong spectral difference between diseased and healthy peach fruits. (II) shows the classification results for mildly diseased, where the experimental group by inoculation *B.cinerea* had quite poor classification results, with only 41% classification accuracy of the spectral information. The classification accuracy gradually increased with increasing rot. Compared with the classification results of the “severe rot” stage, the “slight” and “average” rot had a higher misclassification rate. This suggests that it is difficult to differentiate between the three diseases based on spectra at the light rot stage because the symptoms of the different diseases are not shown at the early stage of the disease. Similar to the modeling approach based on the full spectral wavelength range, the modeling results based on image features are shown in Table (B). The performance of the modeling based on image features was poor compared to the modeling based on spectral information. It is difficult to clearly distinguish the differences between the three fungal diseases from the images, while the spectral information reflects more some physicochemical properties inside the samples is more effective in the differentiation of the different diseases. According to the results in (B), healthy peaches were easy to recognize, with recognition accuracy of 100% at all levels except for the slight decay stage, where the accuracy was 95% and 91%. In the severe decay stage, the results of image feature classification were not as good as those of the spectral model, indicating that image features are limited in classification applications. In order to improve the classification accuracy, the spectral and image information of hyperspectral images were fully utilized, and the PLS-DA model was investigated by combining the integrated information of spectra and images. (C) shows that the model based on the integrated information, exhibits good performance, especially in the full stage, and its accuracy has a more significant growth rate, and the mean recognition accuracy of the modeling set and the validation set are 93.733% and 85.824%, respectively. In general, sufficient information can show better classification accuracy, thus proving that data merging in the current work is feasible for extracting hyperspectral image features. The results show that it is very difficult to distinguish the three diseases at the mild stage of decay, and that spectral and image information can be used to recognize them effectively in severely decayed peach fruits, even though it is difficult to classify the three diseases with the naked eye.

Table 3. The results of the results of the PLS-DA model of the different disease levels

Level	Species	(A)Spectral feature		(B)Image feature		(C)Spectrum + image	
		MS	VS	MS	VS	MS	VS
(Ⅰ) Whole	B.c	73.455	70	86.622	83.345	88.266	83.321
	C.a	93.452	86.422	83.315	66.636	92.532	63.322
	R.s	96.631	90.456	90.452	76.632	94.133	96.652
	Health	100	90.455	100	100	100	100
	Subtotal	**90.885**	84.333	**90.097**	81.653	**93.733**	85.824
(Ⅱ) Slight	B.c	56	41	98	65	56.254	54
	C.a	94	83	76	45	94	82
	R.s	67	75	81	91	97	95
	Health	98	95	95	91	96	97
	Subtotal	78.75	73.5	87.5	73	85.814	82
(Ⅲ) Normal	B.c	76	75	100	85	75.824	98
	C.a	91	83	79	72	86.631	95
	R.s	98	98	91	63	100	81
	Health	100	100	100	100	100	100
	Subtotal	91.25	89	92.5	80	90.614	93.5
(Ⅳ) Serious	B.c	84.665	91	100	85	90	90
	C.a	85.216	85	98	85	86.125	95
	R.s	100	93	96	72	95	100
	Health	95	100	100	100	100	100
	Subtotal	91.22	92.25	98.5	85.5	92.781	96.25

3.3.5. Application of Food Testing Technology in Food Safety Regulation. The application of spectroscopic detection technology in food safety testing is becoming more and more extensive and in-depth, providing strong technical support for food safety. This technology mainly analyzes the spectral information in food to quickly and accurately identify the ingredients, pollutants and harmful substances in food, so as to protect the public's dietary safety. Spectroscopic detection technology is based on the specific spectral features generated when a substance interacts with light, and the composition and structure of the substance can be inferred by measuring these spectral features. Common spectroscopic detection methods include infrared spectroscopy, Raman spectroscopy, ultraviolet-visible absorption spectroscopy and hyperspectral imaging. Each of these techniques has its own characteristics and can be applied to different food safety testing scenarios.

Spectral detection techniques can be applied to food freshness detection. For example, real-time monitoring of the appearance and internal composition information of food through hyperspectral imaging technology can assess the freshness and ripeness of food. In foods such as fruits and meats, the technology is able to detect the degree of spoilage and ripeness, helping consumers and producers to make rational purchasing and storage decisions. In addition, the spectral detection technology is able to identify pathogenic bacteria in food, such as Salmonella and E. coli. By detecting the characteristics of these microorganisms, food safety hazards can be detected in time to protect public health.

Spectral detection technology can also be used to detect pesticide residues and illegal additives in food. These harmful substances pose a potential threat to human health, and spectral detection can achieve rapid and accurate screening, providing strong support for food safety regulatory authorities. Combining hyperspectral imaging technology and chemometric methods, a food traceability system can be established. By analyzing the spectral differences of agricultural products from different origins, an analytical map of the product's origin can be established to ensure that the quality and safety of food can be traced.

4. Conclusion

In this paper, deep learning models are used to recognize the color, size and fruit shape of peach fruits, and combined with near-infrared spectral detection technology to quantitatively predict the ripeness of peach fruits. The associative convolutional neural network structure and YOLO target detection algorithm are used to realize disease detection on peach fruits.

1) The measured values of SSC ranged from 10.615% to 16.425%, and the predicted values ranged from 11.268% to 16.185%. The measured mean and standard deviation of fruit size were 6.016 and 2.755, respectively, and the predicted mean was 4.763 with a standard deviation of 2.036. Through preliminary observation, the distribution of measured and predicted values of quality parameters was similar.

2) Using near-infrared spectroscopy to detect peach fruit ripeness, in the 4500-8500 cm^{-1} wave number, the absorbance has a great difference, in the 5000 cm^{-1} wave number, the absorbance in the 0.9-0.9935 or so, and 6750 cm^{-1} wave number, the absorbance is in the range of 0.745-0.806. This is due to the peach internal quality of different degrees of change caused by.

3) The combination of spectral and image feature processing techniques, especially in all stages, has a more significant growth rate of accuracy, and the mean recognition accuracy of the modeling set and the validation set are 93.733% and 85.824%, respectively.

References

[1] Minas, I. S., Tanou, G., & Molassiotis, A. (2018). Environmental and orchard bases of peach fruit quality. Scientia Horticulturae, 235, 307-322.

[2] Anthony, B. M., & Minas, I. S. (2022). Redefining the impact of preharvest factors on peach fruit quality development and metabolism: A review. Scientia Horticulturae, 297, 110919.

[3] Zhang, G., Fu, Q., Fu, Z., Li, X., Matetić, M., Brkic Bakaric, M., & Jemrić, T. (2020). A comprehensive peach fruit quality evaluation method for grading and consumption. Applied Sciences, 10(4), 1348.

[4] Reig, G., Cisneros-Zevallos, L., Costa, G., & Crisosto, C. H. (2023). Peach fruit quality: Components, composition, and nutritional and health benefits. In Peach (pp. 226-260). GB: CABI.

[5] Hayat, U., Li, W., Bie, H., Liu, S., Guo, D., & Cao, K. (2023). An overview on post-harvest technological advances and ripening techniques for increasing peach fruit quality and shelf life. Horticulturae, 10(1), 4.

[6] Wang, D., Ding, C., Feng, Z., & Cui, D. (2020). A low-cost handheld apparatus for inspection of peach firmness by sensing fruit resistance. Computers and Electronics in Agriculture, 174, 105463.

[7] Minas, I. S., Anthony, B. M., Drogoudi, P., & Costa, G. (2023). Non-Destructive Peach Fruit Maturity and Quality Assessment. In Peach (pp. 175-205). GB: CABI.

[8] Wang, Y., Gu, H. W., Yin, X. L., Geng, T., Long, W., Fu, H., & She, Y. (2024). Deep leaning in food safety and authenticity detection: An integrative review and future prospects. Trends in Food Science & Technology, 104396.

[9] Akbar, M., Ullah, M., Shah, B., Khan, R. U., Hussain, T., Ali, F., ... & Kwak, K. S. (2022). An effective deep learning approach for the classification of Bacteriosis in peach leave. Frontiers in plant science, 13, 1064854.

[10] Rong, D., Wang, H., Ying, Y., Zhang, Z., & Zhang, Y. (2020). Peach variety detection using VIS-NIR spectroscopy and deep learning. Computers and Electronics in Agriculture, 175, 105553.

[11] Luo, D., Luo, R., Cheng, J., & Liu, X. (2024). Quality detection and grading of peach fruit based on image processing method and neural networks in agricultural industry. Frontiers in Plant Science, 15, 1415095.

[12] Chhetri, K. B. (2024). Applications of artificial intelligence and machine learning in food quality control and safety assessment. Food Engineering Reviews, 16(1), 1-21.

[13] Zhou, L., Zhang, C., Liu, F., Qiu, Z., & He, Y. (2019). Application of deep learning in food: a review. Comprehensive reviews in food science and food safety, 18(6), 1793-1811.

[14] Chen, T. C., & Yu, S. Y. (2021). Research on food safety sampling inspection system based on deep learning. Food Science and Technology, 42, e29121.

[15] Han, J., Li, T., He, Y., & Gao, Q. (2022). Using machine learning approaches for food quality detection. Mathematical Problems in Engineering, 2022(1), 6852022.

[16] Lin, Y., Ma, J., Wang, Q., & Sun, D. W. (2023). Applications of machine learning techniques for enhancing nondestructive food quality and safety detection. Critical Reviews in Food Science and Nutrition, 63(12), 1649-1669.

[17] Ismail, N., & Malik, O. A. (2022). Real-time visual inspection system for grading fruits using computer vision and deep learning techniques. Information Processing in Agriculture, 9(1), 24-37.

[18] Li, Y., Man, S., Ye, S., Liu, G., & Ma, L. (2022). CRISPR-Cas-based detection for food safety problems: Current status, challenges, and opportunities. Comprehensive Reviews in Food Science and Food Safety, 21(4), 3770-3798.

[19] Alosaimi, W., Alyami, H., & Uddin, M. I. (2021). PeachNet: Peach Diseases Detection for Automatic Harvesting. Computers, Materials & Continua, 67(2).

[20] Masuda, K., Uchida, R., Fujita, N., Miyamoto, Y., Yasue, T., Kubo, Y., ... & Akagi, T. (2023). Application of deep learning diagnosis for multiple traits sorting in peach fruit. Postharvest Biology and Technology, 201, 112348.

[21] Qi, H., Luo, J., Wu, X., & Zhang, C. (2024). Application of nondestructive techniques for peach (Prunus persica) quality inspection: A review. Journal of Food Science, 89(11), 6863-6887.

[22] Huang, S., Zhou, G., He, M., Chen, A., Zhang, W., & Hu, Y. (2020). Detection of peach disease image based on asymptotic non-local means and PCNN-IPELM. IEEE Access, 8, 136421-136433.

[23] Yao, N., Ni, F., Wu, M., Wang, H., Li, G., & Sung, W. K. (2022). Deep learning-based segmentation of peach diseases using convolutional neural network. Frontiers in Plant Science, 13, 876357.

[24] Shi, G., & Li, N. (2024). Building an Intelligent Food Safety Inspection System Based on the Internet of Things. Journal of Information Processing Systems, 20(5), 654-662.

[25] Qin, J., Hong, J., Cho, H., Van Kessel, J. A. S., Baek, I., Chao, K., & Kim, M. S. (2023). A multimodal optical sensing system for automated and intelligent food safety inspection. Journal of the ASABE, 66(4), 839-849.

[26] Aslam, H. K. W., Aslam, F., Aleem, M., Iqbal, Z., Khalid, S., Firdous, N., ... & Ali, M. (2024). AI-driven food safety: transforming food inspection, traceability, and compliance in food industry and regulatory bodies: A mini review. Food Science & Applied Microbiology Reports, 3(2), 61-67.

[27] Qian, C., Murphy, S. I., Orsi, R. H., & Wiedmann, M. (2023). How can AI help improve food safety?. Annual Review of Food Science and Technology, 14(1), 517-538.

[28] Wu, M., Liu, W., & Zheng, S. (2024). Intelligent food safety: a prediction model based on attention mechanism and reinforcement learning. Applied Artificial Intelligence, 38(1), 2379731.

[29] Jiacong Ping,Nan Hao,Xuting Guo,Peiqi Miao,Zhiqi Guan,Haiyang Chen.& Wenlong Li. (2025). Rapid and accurate identification of Panax ginseng origins based on data fusion of near-infrared and laser-induced breakdown spectroscopy. Food Research International115925-115925.

[30] Yifan Wu,Silong Peng,Qiong Xie,Quanjie Han,Genwei Zhang & Haigang Sun. (2019). An improved weighted multiplicative scatter correction algorithm with the use of variable selection: Application to near-infrared spectra. Chemometrics and Intelligent Laboratory Systems114-121.

[31] Wenliang Pan,Yue Shan,Chuang Li,Shuai Huang,Tengfei Li,Yun Li & Hongtu Zhu. (2024). FPLS-DC: Functional partial least squares through distance covariance for imaging genetics. Bioinformatics (Oxford, England).